This is the Pre-Published Version.

Y. Zeng, Y. Li, P. Du, X. Huang (2023) *Smart Fire Detection Analysis in Complex Building Floorplans Powered by GAN*, **Journal of Building Engineering**, 107858. https://doi.org/10.1016/j.jobe.2023.107858

Smart Fire Detection Analysis in Complex Building Floorplans Powered by GAN

Yanfu Zeng[1], Yizhou Li[1], Peilun Du[2], Xinyan Huang[1,2,*]

[1]*Dept. of Building Environment and Energy Engineering, Hong Kong Polytechnic University, Hong Kong*

[2]*The Hong Kong Polytechnic University Shenzhen Research Institute, Shenzhen, China*

**Corresponding to xy.huang@polyu.edu.hk (XH)*

Abstract:

Ceiling-mounted fire service systems are the most widely used provisions to ensure building fire safety. The current design distribution of fire detectors is based on semi-empirical correlations derived from open-floor fire experiments, but the building floorplan affects their activation. This work develops a generative adversarial network (GAN) model to achieve accurate and real-time fire detection analysis for buildings with complex floorplans. A numerical fire database with hundreds of floorplans, fire locations and ceiling heights is established to train the GAN model. The pre-trained model can recognize the geometric characteristics and reveal the fire dynamics laws. Given any building floorplan and fire detector distribution, the model can predict ceiling temperature, velocity and soot density fields with an accuracy of 88% in a second and detection time with 95% accuracy. The proposed GAN model enables a smart fire detection analysis, reduces the fire engineering design cost, and improves fire safety for complex buildings.

Keywords: *AI; Smart Firefighting; Building Fire Simulation; Fire Detection; Fire Safety Design.*

Graphic Abstract:

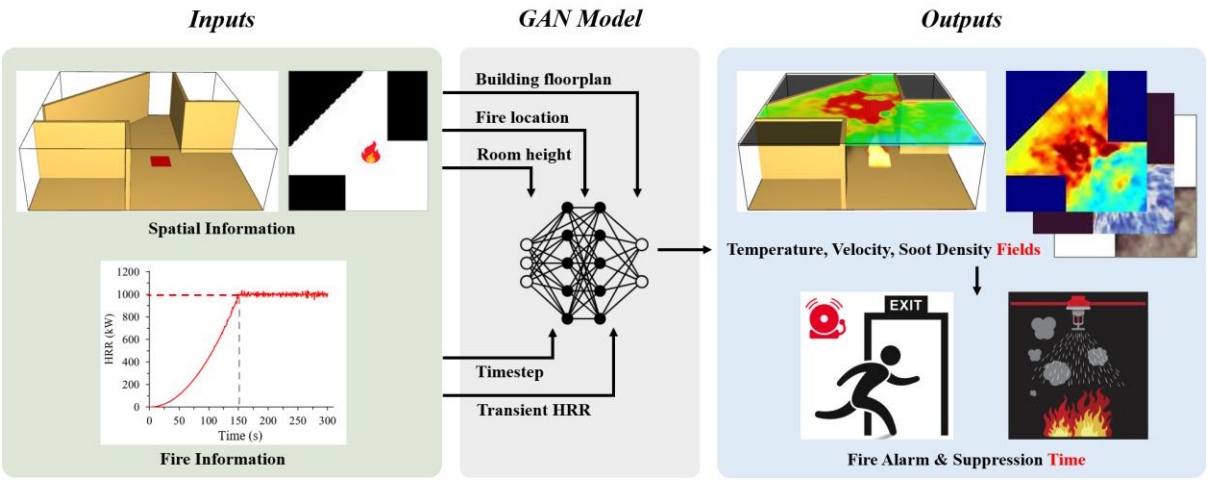

Abbreviations

AI	artificial intelligence	HRR	heat release rate
ASET	available safe egress time	LES	large eddy simulation
CFD	computational fluid dynamics	MAE	mean absolute error
CNN	convolutional neural network	PBD	performance-based design
FDS	fire dynamics simulator	RTI	response time index
GAN	generative adversarial networks	RSET	required safe egress time

1. Introduction

Fire detectors (e.g., smoke and heat detectors) and water-based fire suppression systems (e.g., sprinkler, water mist) are key components to ensure building safety under fire situations. They are commonly seen in almost every modern building. In case of a building fire, burning will generate massive hot and toxic smoke that floats up driven by the buoyancy force [1]. Then, a hot smoke layer forms up and accumulates on the ceiling, which propagates horizontally to other rooms (i.e., a smoke ceiling jet) and also descends vertically from the ceiling to the floor. Therefore, the detectors and sprinklers are normally mounted below the ceiling, aiming to get an early response when the fire smoke ceiling jet arrives.

In most countries, design relaxations are always granted if the building is sprinkler protected, such as the less required smoke extraction capacity, larger allowed building volume/height, longer permitted travel distance, relaxer tenability criteria selection, etc. [2–5], which demonstrates the importance of the sprinkler system. Therefore, the analysis of detector/sprinkler activation is always performed in the building fire engineering design process. On the one hand, the sprinkler is expected to control the fire development after it activates. Specifically, the maximum fire HRR for design consideration could be the value when the sprinkler activates [6] (Fig. 1a). If the estimated detection time, i.e., the duration between the fire ignition and the moment when the fire detector senses the fire occurrence, is longer, the considered design fire is more severe, resulting in a less Available Safety Egress Time (ASET). On the other hand, the detection time of the fire detector is one of the deterministic elements of Required Safe Egress Time (RSET) [7], which is established to assess the human evacuation process. The timeline analysis by comparing ASET and RSET, as shown on the right side of Fig. 1a, is the most standard criteria in terms of life safety protection in the Performance-based Design (PBD) of building fire safety.

The detector/sprinkler activation mainly depends on two attributes based on the heat transfer equation proposed by Heskestad and Smith [8] (Eq. 1). The first attribute is the thermal properties of the product, i.e., Response Time Index (RTI) and activation temperature. There are several standard values regulated by the industry, e.g., an RTI of 80 $m^{1/2} \cdot s^{1/2}$ and an activation temperature of 68 °C. The second attribute is the ceiling jet features, i.e., temperature and velocity, exposed to the detector/sprinkler under fire situation.

$$\Delta T_d = T_{d,n} - T_{d,n-1} = \frac{V_n^{1/2}(T_{g,n} - T_{d,n-1})}{RTI}\Delta t \quad (1)$$

where ΔT_d is the temperature rise of the device, °C; $T_{d,n}$ is the device temperature at time step n, °C; $T_{d,n-1}$ is the device temperature at time step (n-1), °C; V_n is the gas velocity at time step n, m/s; $T_{g,n}$ is the gas temperature at time step n, m/s; RTI is the response time index of the device, $m^{1/2}{\cdot}s^{1/2}$; and Δt is the time interval, s.

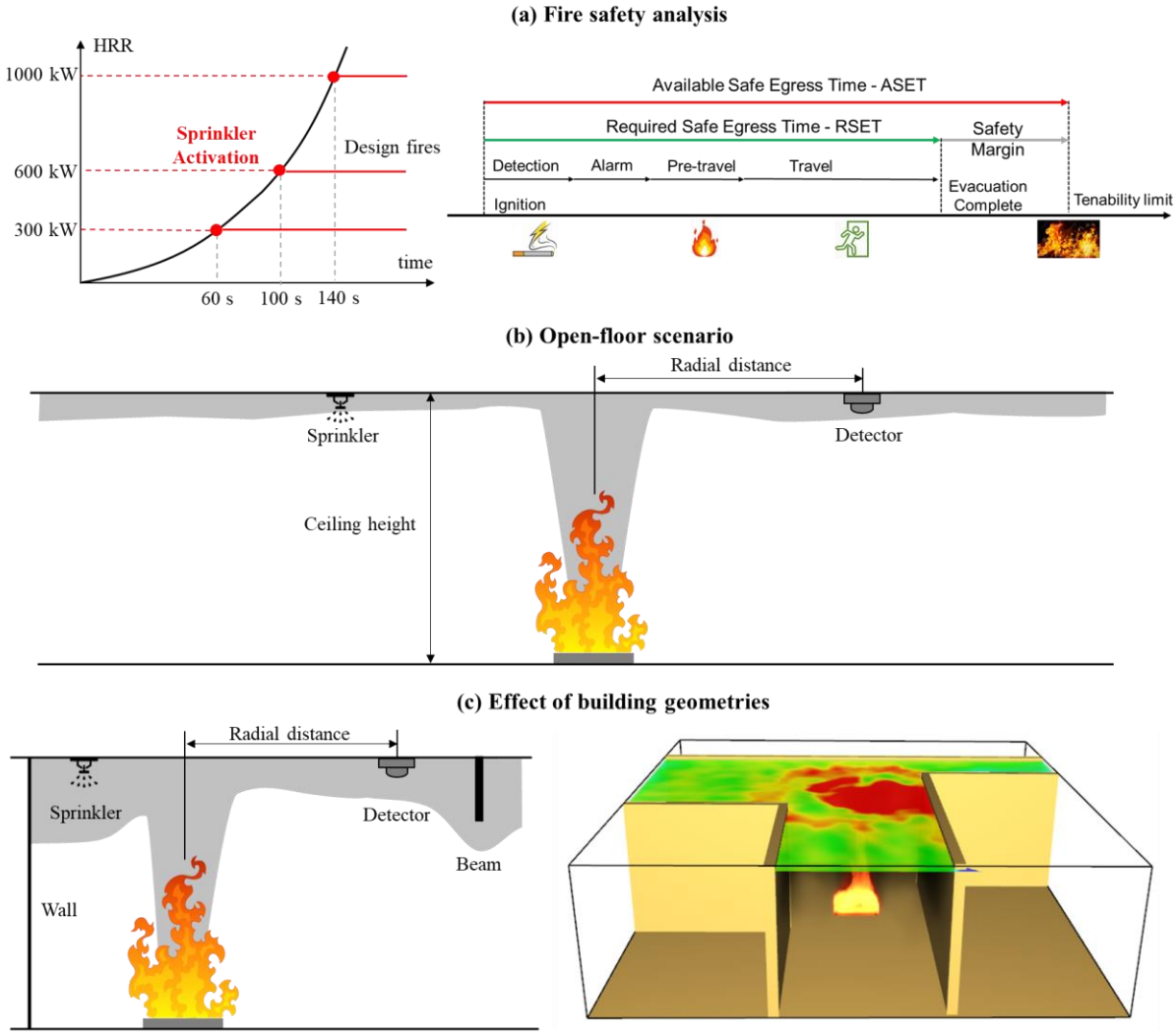

Fig. 1. (a) Fire safety analysis corresponding to detection time; (b) simplified open-floor scenario addressed in most empirical models; and (c) smoke layer accumulation caused by building structures.

Today, the prediction of ceiling jet features still relies on semi-empirical correlations [9–11], such as Alpert's correlations (Eqs. 2-3), which estimate the ceiling temperature and velocity based on the information about HRR, ceiling height, and radial distance (Fig. 1b).

$$T - T_\infty = 5.38\frac{\dot{Q}^{2/3}/H^{5/3}}{(r/H)^{2/3}} \quad (2)$$

$$V = 0.197\frac{(\dot{Q}/H)^{1/3}}{(r/H)^{5/6}} \quad (3)$$

where T is the gas temperature in ceiling jet flow, °C; V is the total velocity in ceiling jet flow, m/s; T_∞ is the ambient temperature, °C; $\dot{Q}$ is the heat release rate (HRR), kW; r is the horizontal distance to the fire centreline, m; and H is the height between ceiling and fuel surface, m.

Due to their simplicity, those correlations are widely adopted in fire engineering analysis of detector activation, but their applicability in realistic fire scenarios is often questioned. For example, Alpert's semi-empirical correlations are derived from the steady-burning fire test data with an open-floor ceiling [11] (Fig. 1b). However, a realistic fire varies with time, especially at the early fire stage when the detection system is expected to operate [12]. As for the functional relationships proposed by Heskestad and Delichatsios [10], although they address the T-square growing fire situation, the reported error between calculated data and actual data can be up to 50% [13,14].

The most significant discrepancy between the correlation-addressed scenario and realistic fire situation is, however, the simplicity of the building structures. The existence of the structure elements, e.g., walls, rooms, corridors and corners, has considerable impacts on the temperature, (total) velocity, and smoke density distributions below the ceiling (Fig. 1c). Past research only addresses the unconfined fire conditions [11,12,15–17], where the surrounding boundaries of the fire are fully opened like the first picture in Fig. 1b. Some of them have further investigated the effect of walls to the ceiling jet features [18,19]. Nevertheless, they are still limited to describing the simplistic rectangular room shape or a straight corridor.

Computational Fluid Dynamics (CFD) modelling [20] is another feasible approach to overcome the abovementioned limitations. It can reproduce the fire gas development under complex fire scenarios with growing fire situations and the given building floorplan. Nevertheless, it is rarely used in design practices simply because of its high computational cost. For example, modelling a fire development of 20 min usually requires a computational time of 48 hours with a 32-core server. So far, there is no feasible approach to provide both accurate and prompt fire detection analysis for a given floorplan.

Artificial Intelligence (AI) methods, especially deep learning algorithms, could be a solution to overcome the abovementioned challenges. There have been many AI applications in building research in recent years, including building design [12,21–33], fire identification [34–37], fire evolution forecasting [38–41], damage detection [42–44], structure fire resilience [45–47], etc. The AI has been approved to be able to provide fire temperature images which are comparable to the CFD modelling.

This work aims to achieve a smart fire detection analysis in complex building structures by using deep learning method. A generative adversarial networks (GAN) model is trained by a CFD numerical database with various building floorplans. The accuracy and efficiency of the model are demonstrated in new floorplans, and the associated detection analysis based on the GAN predictions is performed.

2. GAN model construction

2.1. Database preparation

The first step towards the smart fire detection analysis is to prepare sufficient fire data which deep learning model can learn from. It is, however, difficult to collect such an amount of experimental data due to high expense. Therefore, a numerical database was prepared with CFD fire simulations. These simulations were performed by using Fire Dynamic Simulator (FDS) version 6.7.7 [48]. The following variables are considered when constructing the database because of their significant influences on the ceiling jet features:

(1) **Building floorplan.** Since the prior expectation of the deep learning model in this study is to predict the detector response for an arbitrary building floorplan given by the designer, 34 different floorplans are constructed in a computational domain of 10 × 10 m^2, including unconfined space, one-side wall, various-shape corridors, confined rooms, etc. Fig. 2 presents some floorplan examples, and the completed floorplan set is presented in Appendix A.

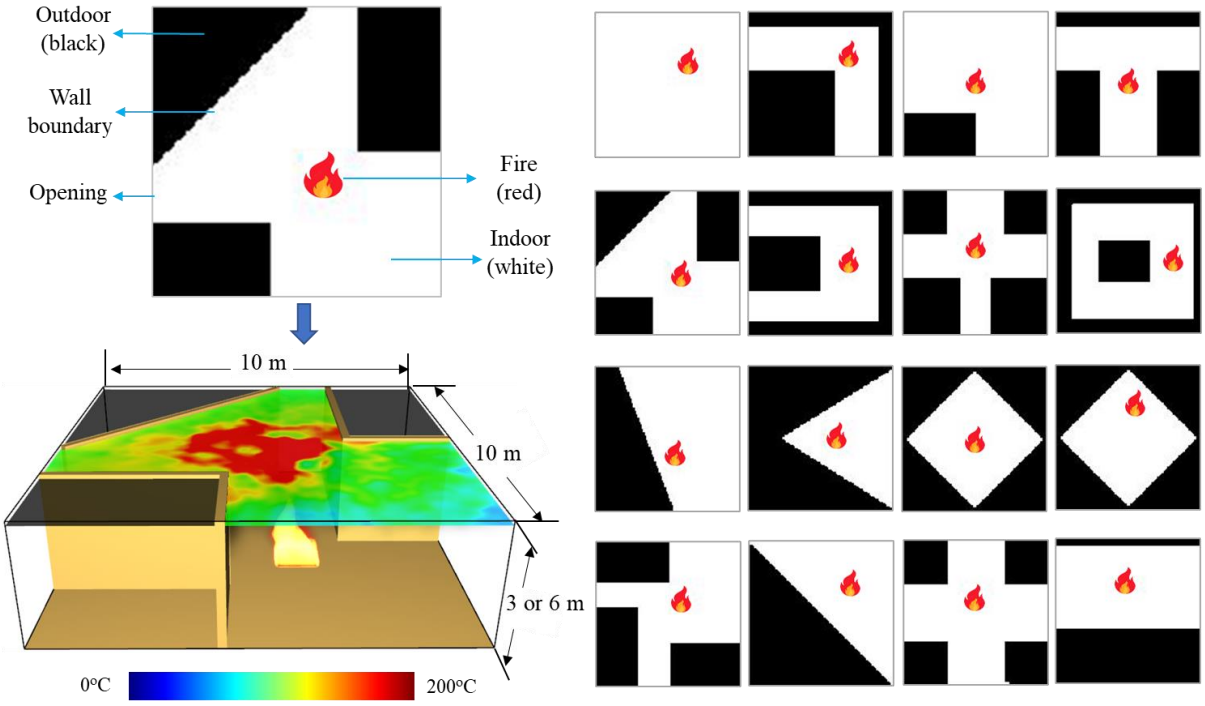

Fig. 2. Examples of the building floorplans in the database, where the fire location (red), indoor space (white) and outdoor area (black) are presented.

(2) **Fire location.** Fire source location is the most dominant attribute of the ceiling temperature/velocity distribution. Thus, for each floorplan, two different fire locations are considered: one is near the wall, and another is away from it.

(3) **Ceiling height.** Ceiling height is another critical attribute of ceiling jet features. While the fire/smoke plume keeps entraining the ambient air during the rising process, the ceiling jet

temperature will be lower with the increase of the ceiling height. Two ceiling heights, i.e., 3 m and 6 m, are studied here, which cover most of the civil buildings.

(4) **Transient fire heat release rate (HRR) at specific timestep**. In this study, t-square (t^2) growth fire is adopted for all simulations, which is representative of the most realistic fires and commonly used in design practices. HRR is set to reach the peak value of 1000 kW at 150 s and remain constant until 300 s, while the ceiling fields evolve accordingly.

(5) **Floor enclosure condition.** If the building has at least one connection to the outdoor area, the smoke layer will reach a stable condition soon after the fire stops growing. In a fully enclosed building, however, the ceiling jet temperature will rise more rapidly due to the smoke accumulation, and it might continue to increase even after the fire HRR remains unchanged.

A total number of 136 fire scenarios were simulated to form the training database. In all the simulations, the ambient temperature is set at 20 °C, and the simulation time is 300 s. The turbulence model uses the Large Eddy Simulation (LES). The radiation is solved by the Optically-Thin model, and fire extinction is controlled by both critical flame temperature and oxygen concentration.

The size of fire source is 1.0 × 1.0 m^2. Ethanol is used as the fuel, while the heat of combustion is 25.6 MJ/kg, and the radiative fraction is 0.26. These fuel properties refer to Alpert's unconfined ceiling jet fire experiments [16], which help to validate the proposed computational settings later. 2-D Z-slices of gas temperature, total gas velocity, and soot density are set at one mesh below the ceiling to collect the interested data for model training.

The cell resolution is a crucial setting in FDS to guarantee simulation accuracy. Sensitivity analysis was performed to determine an appropriate cell size. To save computational cost, steady-burning unconfined fires are simulated while the HRR reaches 1 MW at the beginning of the simulation. Fig. A2 (see Appendix A) shows the reduction of the cell size from 0.1 m to 0.05 m has no significant difference in the simulation result, while the computational time can be saved by 75% for the 0.1-m cell case. Therefore, the cell size of 0.1 m is applied for all the fire simulations to speed up the computational process while maintaining accuracy. The total number of cells is 300,000 or 600,000, depending on the ceiling height. The simulations were run on a 32-core server, and the computational time varied from 12 h to 24 h for a single case.

While the performance of AI greatly depends on the data quality, the computational setting of the CFD model was validated by two cases. Fig. 3a compares the predicted radial temperature profiles between Alpert's correlation (Eq. 2) and CFD model under open-floor fire scenarios (Fig. 1b). It is clear that the simulated temperature profile agrees well with the fitted profile. In Fig. 3b, the solid lines indicate the temperature measurements at different radial distances for a corridor fire experiment introduced in [49,50], while the dashed lines are the simulated results with the proposed computational settings. Good agreement can also be found for the one-end corridor scenario. Thus, the data quality of the deep learning model is satisfied.

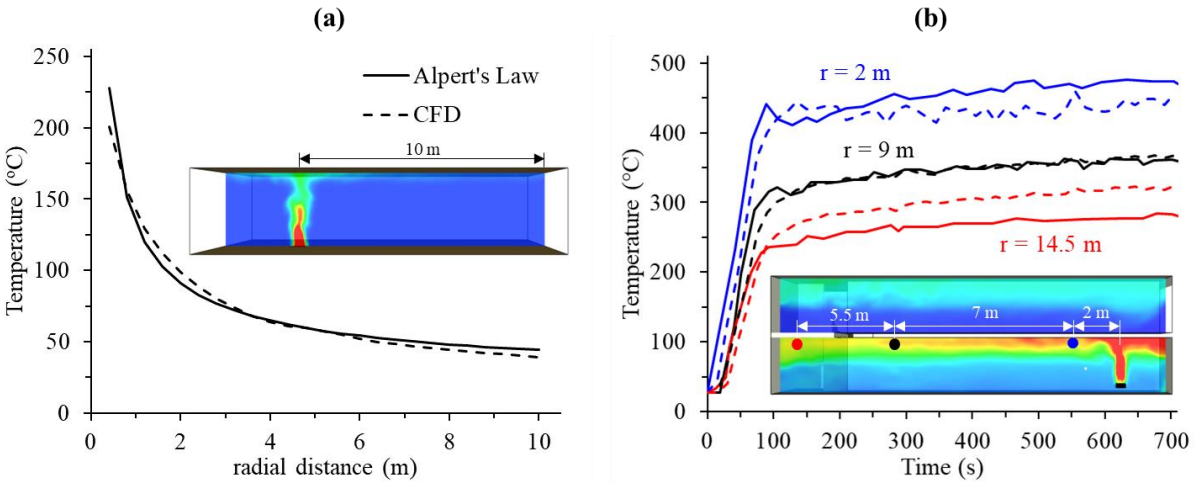

Fig. 3. CFD model validation by (a) Alpert's correlation for an open-floor scenario; and (b) experimental measurements for a corridor fire test (solid line: experiment; dashed line: simulation).

2.2. Data pre-processing and model training

The input of the deep learning model includes two attributes. The first attribute is the spatial information, including the building floorplan and fire location. The spatial information for each case is presented as a 128 × 128 matrix, where the value at the outdoor area, indoor area, and fire position is 0, 1, and 2, respectively (Fig. 4). The second attribute is the design information, including ceiling height, timestep, transient fire HRR, and floor enclosure condition. The transient HRR values and corresponding timesteps were extracted every 10 s. Floorplans are also labelled with 1 if it is enclosed (e.g., sealed room) and 0 if it has openings to the surrounding area (e.g., corridor).

It is noted that the above design information are originally one-dimensional values. For model training purposes, they are also extended to a 128 × 128 matrix, where the value at indoor area is the value of information, and value at outdoor position is still 0. After dimension extension, the design information matrix can be merged with the spatial matrix, which forms an input matrix of 128 × 128 × 5 for model training. The model output is designed as the corresponding ceiling temperature field, velocity field and soot density field, which is presented as an output matrix of 128 × 128 × 3 for model training.

To better evaluate the performance of the proposed generative model, the database is split into training dataset with 102 cases (75%) and testing dataset with 34 cases (25%) (see Appendix A). The training dataset is for model to learn the data correlation and capture the hidden patterns or laws between the design inputs and ceiling jet outputs. The testing dataset is used to quantify the prediction quality once the model is completely trained. To enrich the amount of learning data, the training dataset was augmented by rotating the matrix with the angles of 90°, 180° and 270°, and the number of training data subsequently increased from 102 cases to 408 cases. While each case has 30 data samples (for a 300-s simulation time with data extraction interval of 10 s), the total number of data samples in training dataset is 12,240.

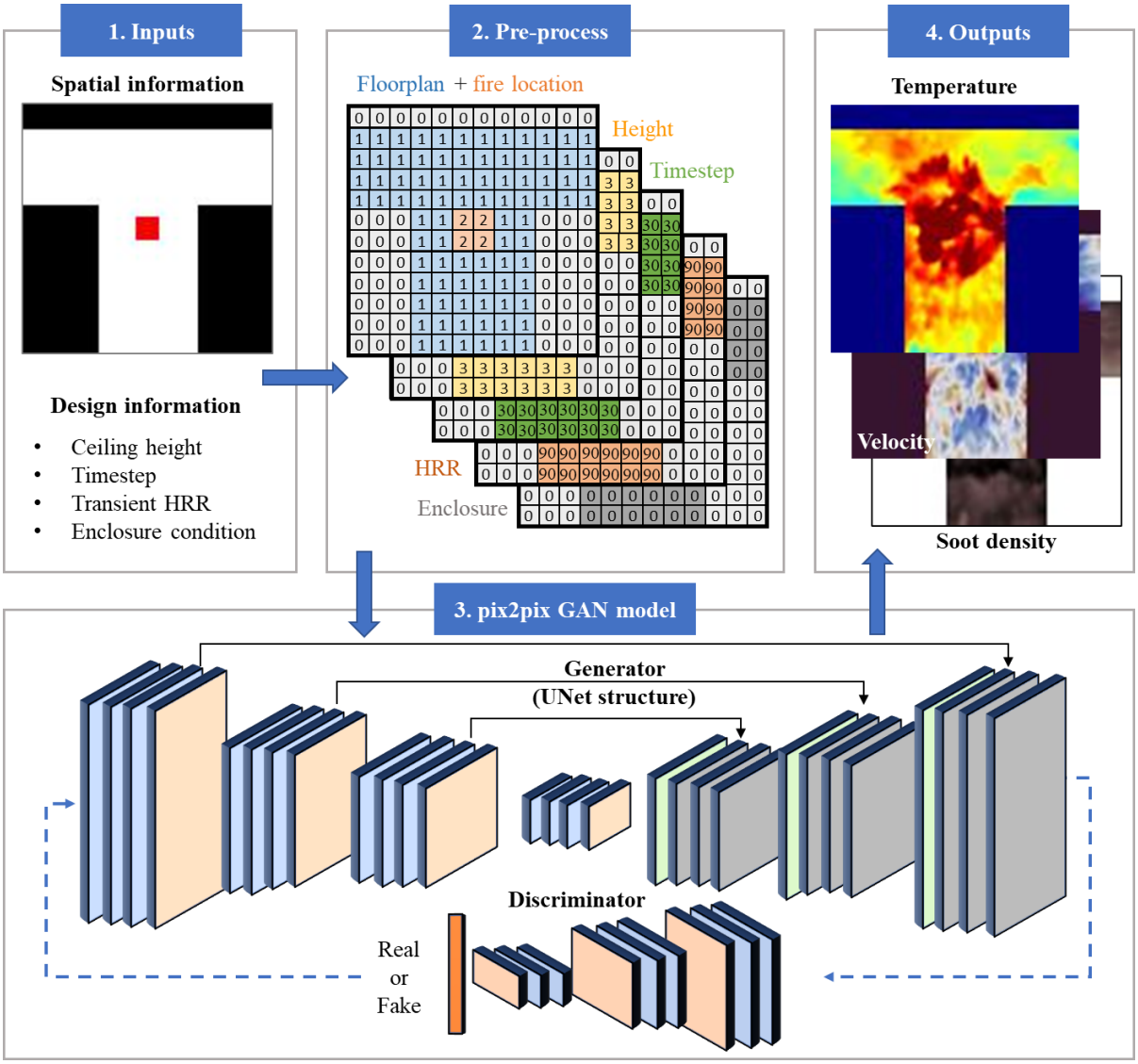

Fig. 4. Details of the model construction.

As for the selection of deep learning algorithm, authors tried both Conventional Neural Networks (CNN)-based algorithms (i.e., traditional CNN, VGG, and UNet) and GAN-based algorithms. Fig. A3 compares the predicted temperature fields between fine-tuned UNet and GAN models. It can be found that GAN model can better reproduce the transient smoke flow patterns with higher accuracy, while the UNet results are prone to be averaged. Thus, the result of GAN-based model with architecture of pix2pix [51] is introduced in the following sections. Specifically, pix2pix GAN model consists of generator and discriminator, as shown in Fig. 5. The generator is established by following the UNet structure. It is responsible for generating fake temperature/velocity outputs that can deceive the discriminator. The discriminator is responsible for distinguishing whether the generated outputs are real or fake and subsequently enhances the performance of generator. The mean absolute error (MAE), defined as the difference between the CFD simulations and AI predictions, was adopted as the loss function of the generator, which can be minimized through number of training iterations. The coefficient of determination R^2 was adopted to illustrate the accuracy of the prediction.

3. Results and discussions

3.1. Model performance

Fig. 5 shows the evolvement of loss and accuracy on training dataset. It can be seen that the model MAE loss reduced quickly at the beginning stage of the training, while no significant improvement can be observed after 80 epochs, indicating that the model has almost converged. The value of MAE loss was minimized to 1.7 after training for 100 epochs. As for the R^2 coefficient, the average value stables at about 88%. Specifically, the R^2 of temperature result is higher than the value of total velocity and soot density, which suggests that the temperature pattern is relatively easier to learn.

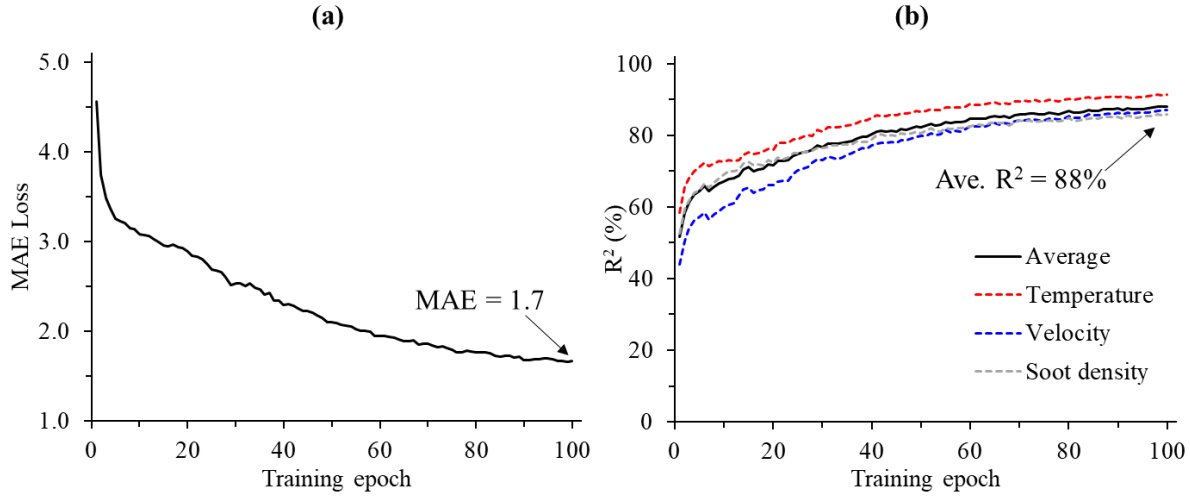

Fig. 5. The evolvements of (a) loss and (b) R^2 with training epochs.

To better demonstrate the prediction quality of the GAN model, Fig. 6 compares the actual (CFD model) and predicted (GAN model) fields of temperature, (total) velocity, and soot density at various timesteps for a complex floorplan, which is never seen by the GAN model during the training process. Video S1 shows their comparisons of three testing cases for the whole 300-s simulation time, and Appendix A summarizes the GAN's predictions on other testing cases. It is noteworthy that it takes only 30 s for GAN model to generate completed 300-s fire images for one case (10 images per second), while it takes 12-24 h for CFD model.

It can be seen that the overall spatial patterns are well learned by the GAN model. It can reproduce the plume region with the highest temperature based on the fire location information provided. The structure boundary is also recognized by the model as well as its physical obstruction to the gas flow. For the left-top area, GAN reproduces the lower temperature distribution because of its good connection to the ambient environment (Fig. 6a). And for the right/bottom side, the narrow structure of the room results in a greater smoke accumulation in these regions, and subsequently increases ceiling temperature in this region. These patterns are all well captured by the GAN model.

On the other hand, the transient fluctuation of the fire is not fully reproduced. Compared to the high-fidelity CFD fire modelling results, the GAN-predicted temperature field is more averaged in each local area, e.g., the left-top side. The prediction of velocity is more challenging than that of temperature

because velocity is a vector, and the magnitude of gas velocity is not sufficient to manifest the direction and pattern of flow. Therefore, the predicted distribution velocity field shows some linear pattern that indicates the overall direction of velocity (see Fig. 6b). This is different from the temperature field which has a circular pattern, i.e., the circular isotherms are formed around the fire centre. Although the overall velocity distribution around fire source is higher than the outer area, the difference is not as high as the temperature. In contrast, the velocity shows greater discrepancy even with the same radial distance to the fire. Nevertheless, the overall velocity prediction quality is still good. Agreement can also be found in soot density results since it has a very similar pattern to the temperature field which is well captured by the GAN model (Fig. 6c).

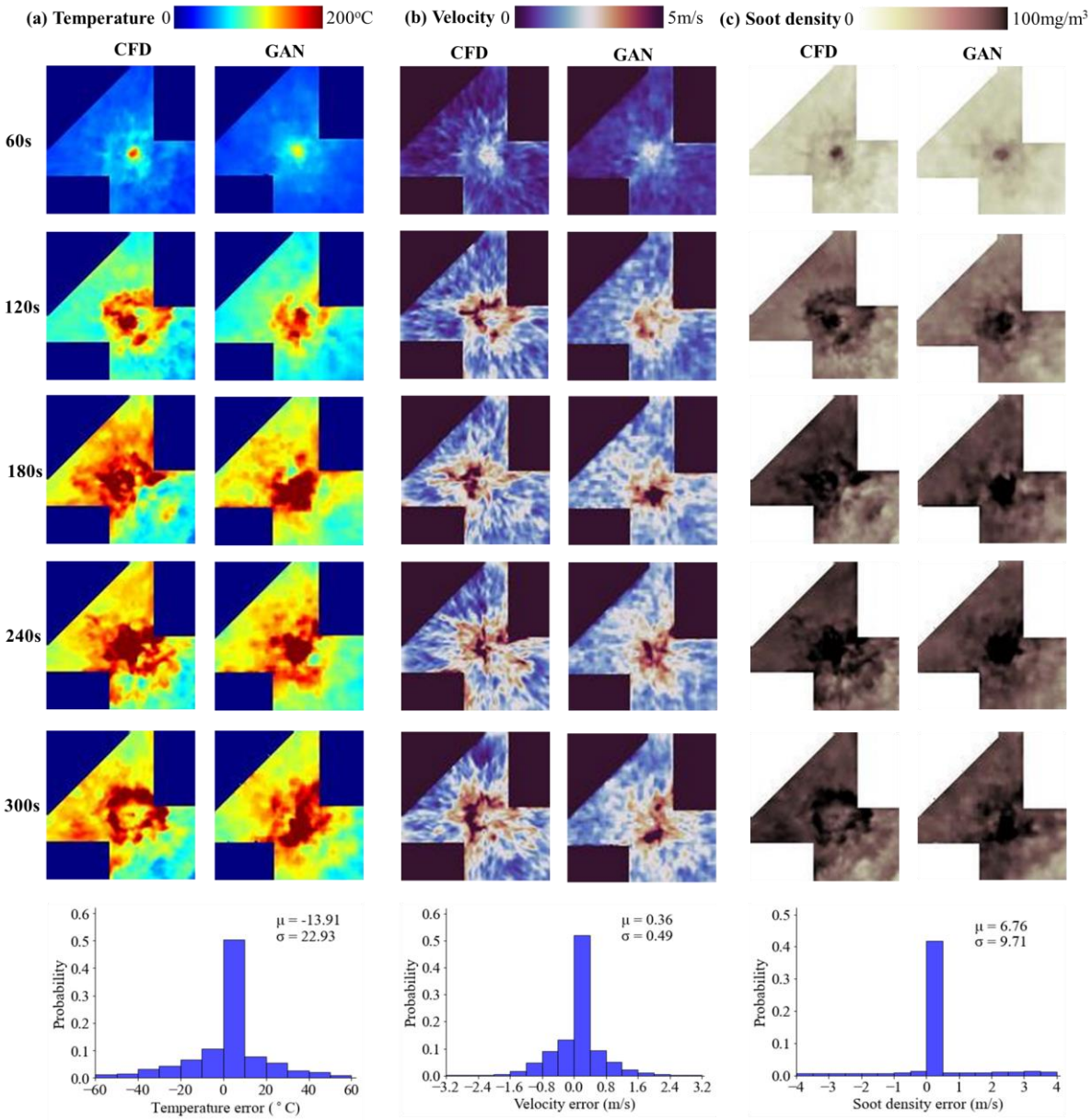

Fig. 6. Comparisons of actual (CFD) and predicted (GAN) ceiling (a) temperature, (b) velocity, and (c) soot density fields at different timesteps with error distribution at 300 s.

To quantify the prediction quality, the mean value (μ) and standard deviation (σ) are calculated for each set of comparisons, and $\mu > 0$ (or $\mu < 0$) means the simulated field is higher (or lower) than the predicted field. The difference distributions are also presented in the last row of Fig. 6. μ and σ of the temperature difference at the end of simulation (300 s) are 13 °C and 23 °C, respectively, and over half of the difference is within 10 °C. Considering the overall ceiling gas temperature is over 200 °C, such a difference is acceptable. As for the velocity, the mean difference is around 0.36 m/s, and the maximum standard deviation is 0.49 m/s. The larger σ could be mainly attributed to that the predicted field is more evenly distributed, while the unsteady flow of the fire gas cannot be fully predicted. This sophisticated nature of convection and turbulent behaviour is challenging for the GAN model to learn without prior expertise knowledge. As for the soot density readings ranging from 0 to around 400 mg/m^3, the mean error of 6.76 mg/m^3 and standard deviation of 9.71 mg/m^3 can be considered as minor differences.

Fig. 7 further compares the evolvement of output fields with different ceiling heights. As expected, the ceiling temperature is significantly reduced with the increase of the ceiling height because of the air entrainment and heat loss to the environment (Fig. 7a). This fire dynamics relationship is also learned by the GAN model, while the predicted results are comparable to the CFD simulation. On the contrary, the overall velocity distribution is slightly higher when the ceiling height increases from 3 m to 6 m (Fig. 7b). It is consistent with the findings in Alpert's research [11]. The soot density follows the same pattern as the temperature, while the smoke is diluted during the process of the plume rising (Fig. 7c). Fig. 7 also presents the temperature and velocity curves at 3 m distance from the fire source, while good agreements can be found between CFD and GAN results for both heights.

As discussed in Section 2.1, the enclosure condition of the building can significantly change the magnitude of ceiling temperature, while it will be much higher if the building is fully enclosed due to smoke accumulation. Authors first trained a GAN model with only 4 inputs (floorplan with fire location, ceiling height, timestep and transient fire HRR). The result shows, however, that the model cannot recognize the enclosure condition automatically. While most of the training cases are connected to the outdoor environment, the predicted temperature still follows their pattern even though the testing building is fully enclosed, as shown in Fig. 8a. Therefore, an additional input of enclosure condition is provided for the model. With this prior knowledge, the model successfully solves the temperature prediction issue for different enclosure conditions. As for the ceiling gas velocity, the smoke accumulation has minor impacts on its evolution (Fig. 8b). Thus, the accuracy improvement for the velocity field is smaller.

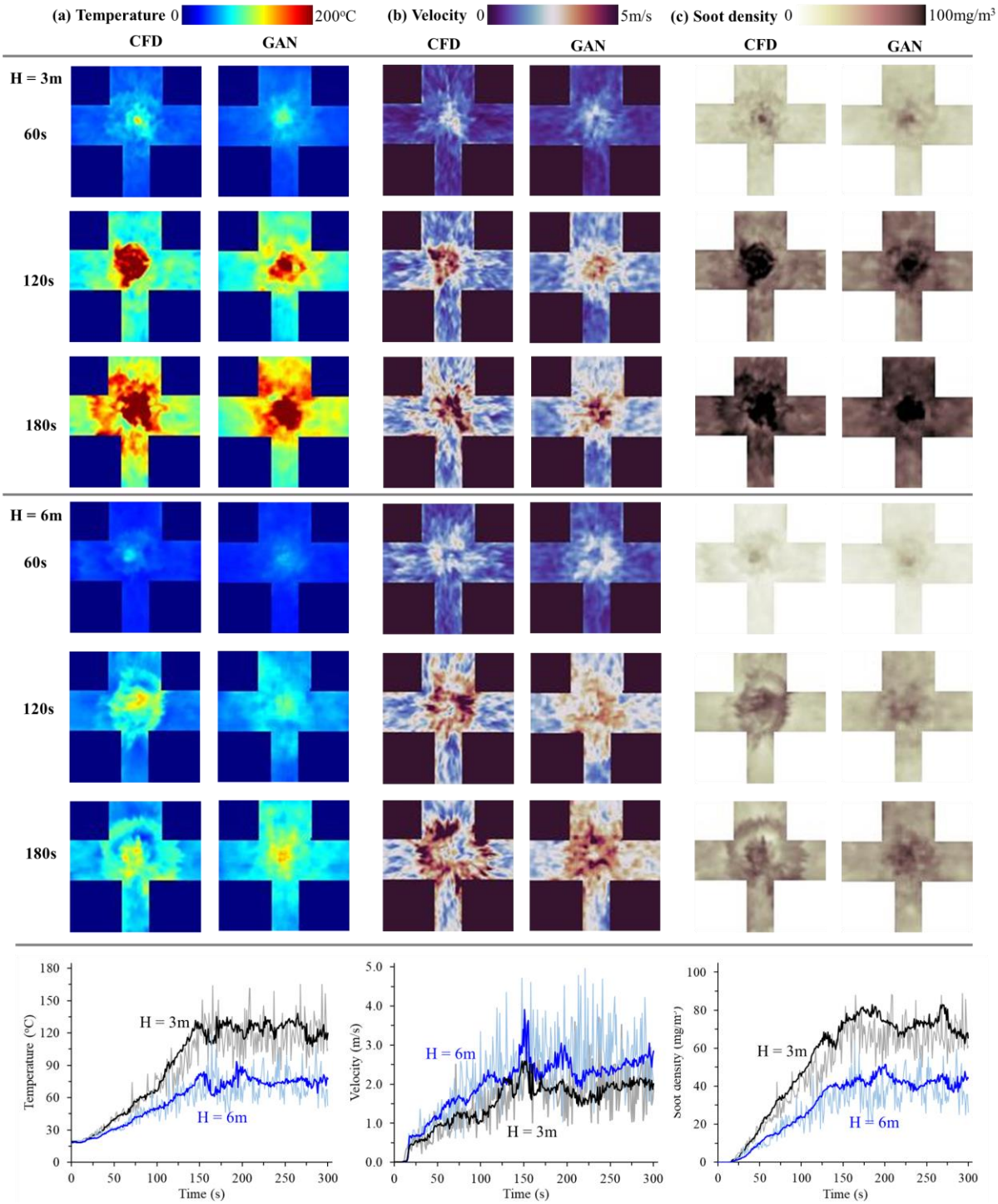

Fig. 7. Effect of ceiling height on (a) temperature, (b) velocity, and (c) soot density fields with profiles at 3 m distance from the fire source, where the lighter lines are CFD model results, and darker lines are GAN model results.

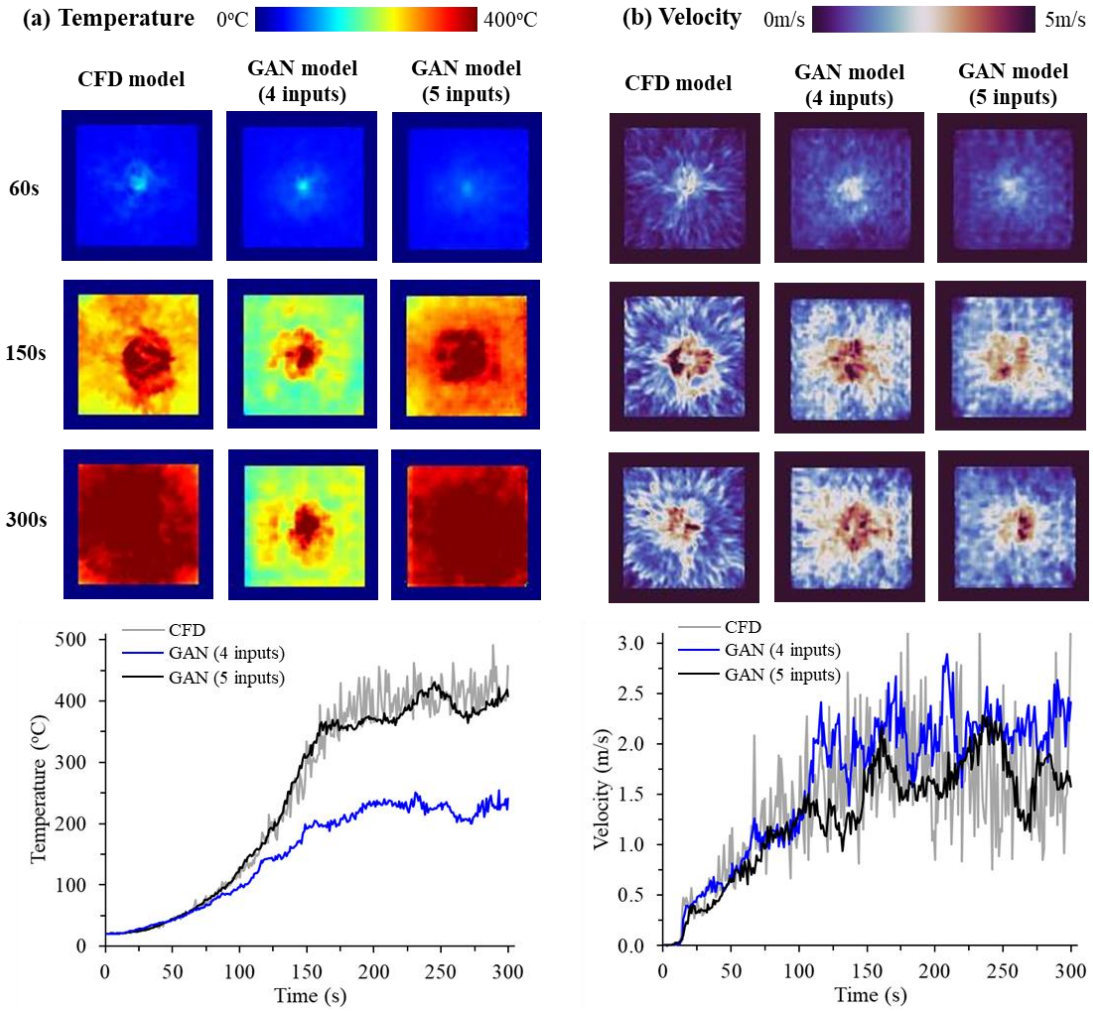

Fig. 8. Effect of the enclosure condition input on GAN model performance: (a) temperature field; and (b) velocity field, with profiles at 3 m distance from the fire source.

3.2. Fire detection analysis

In this section, fire detection analysis for thermal-based devices (i.e., heat detector and sprinkler) is performed to demonstrate the capability of the proposed GAN model. It is a common practice in fire safety design since the result can be the basis of estimating the design fire HRR and evacuation time, as mentioned in Section 1. As for the response of smoke detector, it is less analysed since it usually has a faster response than the thermal devices, and engineers prefer a more conservative analysis to compensate for the design uncertainties. Nevertheless, the model output of soot density can be further processed to estimate the smoke detector response if needed.

A prescriptive design case that complies with the Chinese fire code is proposed [52], where the maximum spacing of sprinklers is 3.6 m for high-rise civil buildings, e.g., office buildings and hotels. Assuming the fire starts at a centre point between the prescriptive-designed sprinklers with a maximum spacing of 3.6 m; thus, the largest horizontal distance between the fire centre and the sprinkler is 2.6 m.

Fig. 9 shows the temperature and velocity rising curves at 2.6 m distance from the fire, which clearly demonstrates the restrictions of the traditional method based on semi-empirical correlations (Eqs. 2-3).

Although the correlation can provide good predictions for the unconfined building (Fig. 9a), it shows a considerable underestimation if there are structure walls near the fire source. For an enclosed room, the ceiling temperature can reach 500 °C with a 1 MW fire, while the fitted result is only 115 °C. In this case, the traditional method will subsequently suggest a longer detection time than the real value. From a safety perspective, it leads to a more conservative design which makes the building safer. From the stakeholder perspective, however, it results in a higher construction cost.

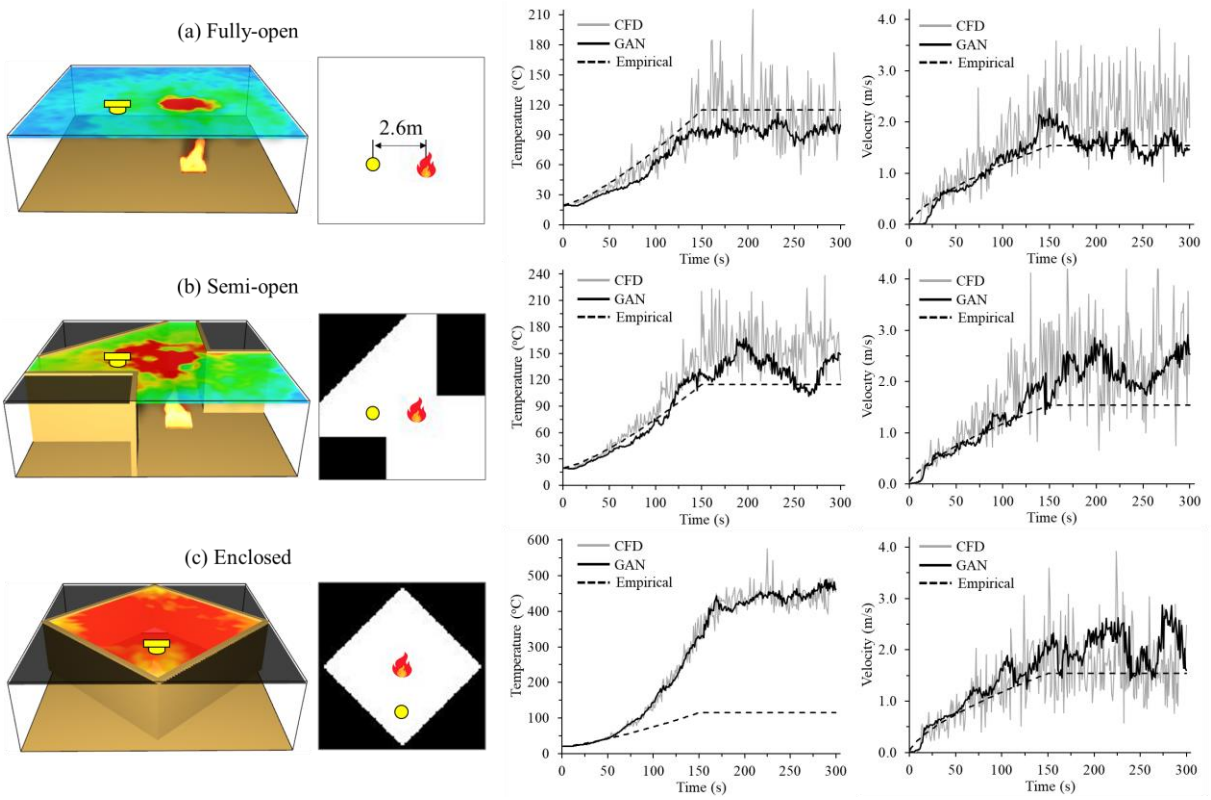

Fig. 9. Evolvement of temperature and velocity at 2.6 m distance from the fire source in (a) unconfined building; (b) partial connected building; and (c) enclosed building.

Fig. 10 shows discrepancies between the actual and predicted detection times for the buildings with a ceiling height of 3 m. While the actual detection times range from 99 to 151 s based on the building floorplan, the traditional method can only provide a fitted result of 147 s with an average error of 17% and maximum error of up to 48%. As for the GAN model, the errors are within 10% in most of the buildings, while the maximum error is 17.2%, and the average error is only 4.6%.

Table 1 compares the traditional methods and proposed smart method for fire detection analysis from different aspects, where the advantages of GAN-driven smart method can be clearly seen. The training of the GAN model is a complex process, but from the users' perspective, they only need to feed the required design information to the pre-trained model instead of fine-tuning the model, which makes it accessible and user-friendly for the engineers. In terms of the cost, the GAN-driven method is comparable to the empirical model, which requires few resources to achieve a real-time analysis, but the accuracy of the detection time prediction can be improved from 83% to 95%, which enables a more

accurate performance assessment on the sprinkler/detection systems.

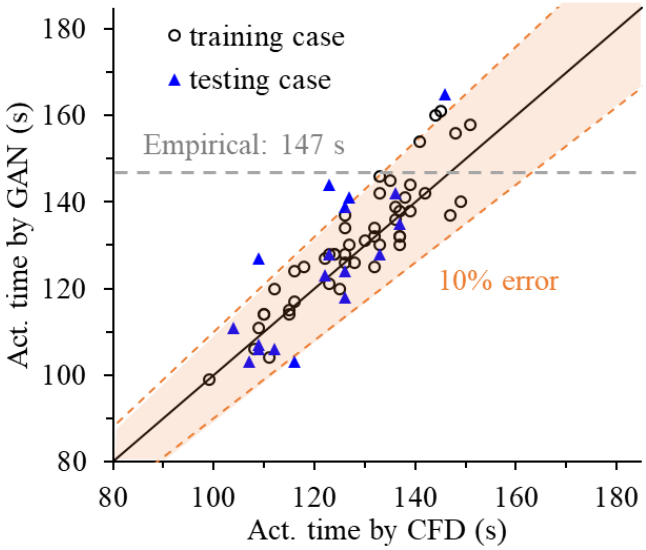

Fig. 10. Comparison of actual (CFD model) and predicted (GAN model and correlation) detection time for buildings with ceiling height of 3 m.

Table 1. Comparison of the traditional methods and proposed smart method from different aspects.

	Empirical method	**CFD method**	**Proposed smart method**
Model complexity	Simple	Complex	Pre-trained
User professional	Low	High	Low
Tool	Spreadsheet	Server	Personal computer
Time	Seconds	12 h	Seconds
Building complexity	Open-floor	Actual	Complex floorplan
Accuracy	83%	Ground truth	95%

To promote the smart fire detection analysis in the industry, there are also some improvements which could be addressed in future work. The first one is to develop an input pre-processing method which can transfer CAD drawings, which is the most commonly used design document, to the spatial matrix needed by the GAN model. Secondly, the current database only contains single corridor/room structures. The demand of handling multiple rooms and corridors is very much needed in practice; thus, representative multi-room cases will be added to the database in the future. The database also needs to be extended with more variables related to fire development, such as fire curves (different growth rates and decay stages), fire source properties (different fuels and smouldering fire), and model outputs (gas concentration and heat flux), in order to meet different design demands.

Another limitation is that the proposed GAN model is only applicable to buildings with flat ceilings. If there is any structure component (e.g., beams) under the ceiling, or the ceiling is declined, the fire gas behaviour can be subsequently changed, and thus, the proposed model is not applicable. One possible solution for this issue is adding another input matrix which contains the information on the

ceiling condition, e.g., the position and depth of the beam and the declined angle of the ceiling, and testing if the model can learn their impacts on the temperature/velocity fields. Moreover, the current model cannot apply to buildings with complex 3-D spatial designs. For example, the building has a balcony in the middle of the space, which obstructs the descending of the smoke layer, or the building shape changes with height, e.g., a pyramid. To address these complex buildings, more sophisticated data processing methods and deep learning architecture are required. Lastly, the current model application is limited to the design analysis, while it has great potentiality to be further applied to the on-site fire detection monitoring, prediction, and forecasting.

4. Conclusions

This study develops a GAN model to enable an accurate and real-time fire detection analysis for buildings having complex floorplans. A numerical fire database was first built with a total of 136 fire simulations to collect fire data, which was subsequently used to train a pix2pix GAN model. By feeding with the information of building floorplan with fire location, HRR pattern, ceiling height, and floor enclosure condition, the proposed GAN model can well recognize the geometric characteristics given by the engineer and reproduce the ceiling temperature, velocity, and soot density fields with 88% accuracy in one second.

These results can be further processed to estimate the detection time with an accuracy of 95%. Compared to the traditional methods based on the empirical models or CFD modelling, the GAN-driven smart method retains good accessibility and low cost while achieving high accuracy, which enables it as the most cost-effective approach so far. In future work, the proposed GAN model could be further upgraded to analyse the fire gas behaviour from a three-dimensional perspective, which helps to address the buildings with more complex shapes.

Data availability

The deep learning algorithm of pix2pix GAN model and training database are available on request.

Acknowledgements

This work is funded by the Hong Kong Research Grants Council Theme-based Research Scheme (T22-505/19-N) and the PolyU Emerging Frontier Area (EFA) Scheme of RISUD (P0013879).

CRediT authorship contribution statement

Yanfu Zeng: Investigation, Methodology, Writing - original draft, Formal analysis.

Yizhou Li: Investigation, Writing - review & editing.

Peilun Du: Methodology, Formal analysis; Resourcing.

Xinyan Huang: Conceptualization, Supervision, Writing - review & editing, Funding acquisition.

References

[1] D. Drysdale, An Introduction to Fire Dynamics, 3rd ed., John Wiley & Sons, Ltd, Chichester, UK, 2011. https://doi.org/10.1002/9781119975465.

[2] Ministry of Housing and Urban-Rural Development of the People's Republic China, GB 51251-2017: Technical standard for smoke management systems in buildings, 2017.

[3] National Fire Protection Association, NFPA 5000: Building Construction and Safety Code, Boston, 2018.

[4] International Code Council (ICC), 2015 IBC International Building Code, International Code Council (ICC), 2014.

[5] Standards New Zealand, NZS 4541: Automatic Fire Sprinkler Systems, Wellington, 2003.

[6] C. Fleischmann, Is Prescription the Future of Performance Based Design?, Fire Safety Science. 10 (2011) 77–94. https://doi.org/10.3801/IAFSS.FSS.10-77.

[7] British Standard Institution, BS 7974:2019 Application of fire safety engineering principles to the design of buildings - Code of practice, BSI Standards Limited, London, 2019.

[8] G. Keskestad, H.F. Smith, Investigation of a New Sprinkler Sensitivity Approval Test: The Plunge Test, FMRC 22485, 1976.

[9] R.P. Schifiliti, R.L.P. Custer, B.J. Meacham, Design of Detection Systems, in: SFPE Handbook of Fire Protection Engineering, Fifth Edition, 2016: pp. 1–3493. https://doi.org/10.1007/978-1-4939-2565-0.

[10] G. Heskestad, M.A. Delichatsios, The initial convective flow in fire, Symposium (International) on Combustion. 17 (1979) 1113–1123. https://doi.org/10.1016/S0082-0784(79)80106-X.

[11] R.L. Alpert, Calculation of response time of ceiling-mounted fire detectors, Fire Technology. 8 (1972) 181–195. https://doi.org/10.1007/BF02590543.

[12] Y. Zeng, X. Huang, Smart building fire safety design driven by artificial intelligence, in: M.Z. Naser (Ed.), InterpretableMachine Learning for the Analysis, Design, Assessment, and Informed DecisionMaking for Civil Infrastructure, Elsevier, New York, 2023. https://doi.org/10.1016/B978-0-12-824073-1.00011-3.

[13] G. Heskestad, M.A. Delichatsios, Environments of fire detectors. Phase 1. Effect of fire size, ceiling height and material, in: National Technical Information Service (NTIS) (Ed.), Volume I: "Measurements" (NBS-GCR-77-86), Springfield, VA, 1977.

[14] R.P. Schifiliti, Use of Fire Plume Theory in the Design and Analysis of Fire Detector and Sprinkler Response, Worcester Polytechnic Institute, 1986.

[15] R.L. Alpert, Turbulent ceiling-jet induced by large-scale fires, Combustion Science and Technology. 11 (1975) 197–213. https://doi.org/10.1080/00102207508946699.

[16] R.L. Alpert, The Fire-Induced Cieling-Jet Revisited, Fireseat. (2011) 1–22.

[17] H.-C. Kung, H.-Z. You, R.D. Spaulding, Ceiling flows of growing rack storage fires, Symposium (International) on Combustion. 21 (1988) 121–128. https://doi.org/10.1016/S0082-0784(88)80238-8.

[18] H. Kurioka, Y. Oka, H. Satoh, O. Sugawa, Fire properties in near field of square fire source with longitudinal ventilation in tunnels, Fire Safety Journal. 38 (2003) 319–340. https://doi.org/10.1016/S0379-7112(02)00089-9.

[19] Z. Gao, H. Wan, J. Ji, Y. Bi, Experimental prediction on the performance and propagation of ceiling jets under the influence of wall confinement, Energy. 178 (2019) 378–385. https://doi.org/10.1016/j.energy.2019.04.138.

[20] G.H. Yeoh, K.K. Yuen, Computational Fluid Dynamics in Fire Engineering, Butterworth-Heinemann,

Burlington, 2009. https://doi.org/10.1016/b978-0-7506-8589-4.00007-7.

[21] Y. Zeng, X. Zhang, L.C. Su, X. Wu, X. Huang, Artificial Intelligence tool for fire safety design (IFETool): Demonstration in large open spaces, Case Studies in Thermal Engineering. 40 (2022) 102483. https://doi.org/10.1016/j.csite.2022.102483.

[22] Y. Fei, W. Liao, Y. Huang, X. Lu, Knowledge-enhanced generative adversarial networks for schematic design of framed tube structures, Automation in Construction. 144 (2022) 104619. https://doi.org/10.1016/j.autcon.2022.104619.

[23] Y. Fei, W. Liao, S. Zhang, P. Yin, B. Han, P. Zhao, X. Chen, X. Lu, Integrated Schematic Design Method for Shear Wall Structures: A Practical Application of Generative Adversarial Networks, Buildings. 12 (2022) 1–17. https://doi.org/10.3390/buildings12091295.

[24] W. Liao, Y. Huang, Z. Zheng, X. Lu, Intelligent generative structural design method for shear wall building based on "fused-text-image-to-image" generative adversarial networks, Expert Systems with Applications. 210 (2022) 118530. https://doi.org/10.1016/j.eswa.2022.118530.

[25] P. Zhao, W. Liao, H. Xue, X. Lu, Intelligent design method for beam and slab of shear wall structure based on deep learning, Journal of Building Engineering. 57 (2022) 104838. https://doi.org/10.1016/j.jobe.2022.104838.

[26] L.C. Su, X. Wu, X. Zhang, X. Huang, Smart performance-based design for building fire safety: Prediction of smoke motion via AI, Journal of Building Engineering. 43 (2021) 102529. https://doi.org/10.1016/j.jobe.2021.102529.

[27] X. Huang, X. Wu, A. Usmani, Handbook of Cognitive and Autonomous Systems for Fire Resilient Infrastructures Chapter 7: Perspectives of Using Artificial Intelligence in Building Fire Safety, n.d.

[28] X. Lu, W. Liao, Y. Zhang, Y. Huang, Intelligent structural design of shear wall residence using physics-enhanced generative adversarial networks, Earthquake Engineering and Structural Dynamics. (2022) 1–20. https://doi.org/10.1002/eqe.3632.

[29] W. Liao, X. Lu, Y. Huang, Z. Zheng, Y. Lin, Automated structural design of shear wall residential buildings using generative adversarial networks, Automation in Construction. 132 (2021) 103931. https://doi.org/10.1016/j.autcon.2021.103931.

[30] W. Liao, X. Wang, Y. Fei, Y. Huang, L. Xie, X. Lu, Base-isolation design of shear wall structures using physics-rule-co-guided self-supervised generative adversarial networks, Earthquake Engineering & Structural Dynamics. (2023) 1–23. https://doi.org/10.1002/eqe.3862.

[31] P. Zhao, W. Liao, Y. Huang, X. Lu, Intelligent design of shear wall layout based on graph neural networks, Advanced Engineering Informatics. 55 (2023) 101886. https://doi.org/10.1016/j.aei.2023.101886.

[32] P. Zhao, W. Liao, Y. Huang, X. Lu, Intelligent design of shear wall layout based on attention-enhanced generative adversarial network, Engineering Structures. 274 (2023) 115170. https://doi.org/10.1016/j.engstruct.2022.115170.

[33] P. Zhao, W. Liao, Y. Huang, X. Lu, Intelligent beam layout design for frame structure based on graph neural networks, Journal of Building Engineering. 63 (2023) 105499. https://doi.org/10.1016/j.jobe.2022.105499.

[34] Z. Wang, T. Zhang, X. Huang, Predicting real-time fire heat release rate by flame images and deep learning, Proceedings of the Combustion Institute. 39 (2023) 4115–4123. https://doi.org/10.1016/j.proci.2022.07.062.

[35] Z. Wang, T. Zhang, X. Wu, X. Huang, Predicting transient building fire based on external smoke images and deep learning, Journal of Building Engineering. 47 (2022) 103823. https://doi.org/10.1016/j.jobe.2021.103823.

[36] T. Zhang, Z. Wang, Y. Zeng, X. Wu, X. Huang, F. Xiao, Building Artificial-Intelligence Digital Fire

(AID-Fire) system: A real-scale demonstration, Journal of Building Engineering. 62 (2022) 105363. https://doi.org/10.1016/J.JOBE.2022.105363.

[37] X. Wu, Y. Park, A. Li, X. Huang, F. Xiao, A. Usmani, Smart Detection of Fire Source in Tunnel Based on the Numerical Database and Artificial Intelligence, Fire Technology. 57 (2021) 657–682. https://doi.org/10.1007/s10694-020-00985-z.

[38] W.C. Tam, E.Y. Fu, J. Li, X. Huang, J. Chen, M.X. Huang, A spatial temporal graph neural network model for predicting flashover in arbitrary building floorplans, Engineering Applications of Artificial Intelligence. 115 (2022) 105258. https://doi.org/10.1016/j.engappai.2022.105258.

[39] T. Zhang, Z. Wang, H.Y. Wong, W.C. Tam, X. Huang, F. Xiao, Real-time forecast of compartment fire and flashover based on deep learning, Fire Safety Journal. 130 (2022) 103579. https://doi.org/10.1016/j.firesaf.2022.103579.

[40] X. Zhang, X. Wu, X. Huang, Smart real-time forecast of transient tunnel fires by a dual-agent deep learning model, Tunnelling and Underground Space Technology. 129 (2022). https://doi.org/10.1016/j.tust.2022.104631.

[41] X. Wu, X. Zhang, X. Huang, F. Xiao, A. Usmani, A real-time forecast of tunnel fire based on numerical database and artificial intelligence, Building Simulation. 15 (2022) 511–524. https://doi.org/10.1007/s12273-021-0775-x.

[42] T. Siriborvornratanakul, Pixel-level thin crack detection on road surface using convolutional neural network for severely imbalanced data, Computer-Aided Civil and Infrastructure Engineering. (2023) 1–17. https://doi.org/10.1111/mice.13010.

[43] P. Bazrafshan, T. On, S. Basereh, P. Okumus, A. Ebrahimkhanlou, A graph-based method for quantifying crack patterns on reinforced concrete shear walls, Computer-Aided Civil and Infrastructure Engineering. (2023) 1–20. https://doi.org/10.1111/mice.13009.

[44] H. Maeda, T. Kashiyama, Y. Sekimoto, T. Seto, H. Omata, Generative adversarial network for road damage detection, Computer-Aided Civil and Infrastructure Engineering. 36 (2021) 47–60. https://doi.org/10.1111/mice.12561.

[45] M.Z. Naser, Mechanistically Informed Machine Learning and Artificial Intelligence in Fire Engineering and Sciences, Fire Technology. 57 (2021) 2741–2784. https://doi.org/10.1007/s10694-020-01069-8.

[46] M.Z. Naser, Fire resistance evaluation through artificial intelligence - A case for timber structures, Fire Safety Journal. 105 (2019) 1–18. https://doi.org/10.1016/j.firesaf.2019.02.002.

[47] Z. NAN, M.A. Orabi, X. Huang, Y. Jiang, A. Usmani, Structural-fire Responses Forecasting via Modular AI, Fire Technology. (2023). https://doi.org/10.1016/j.firesaf.2023.103863.

[48] K. McGrattan, S. Hostikka, R. McDermott, J. Floyd, M. Vanella, Fire Dynamics Simulator User's Guide, NIST Special Publication 1019 Sixth Edition. (2019). https://doi.org/10.6028.

[49] K. McGrattan, S. Hostikka, R. McDermott, J. Floyd, C. Weinschenk, K. Overholt, Fire Dynamics Simulator Technical Reference Guide Volume 3: Validation, 6th ed., National Institute of Standards and Technology (NIST), 2021.

[50] D.T. Sheppard;, B.W. Klein, Burn Tests in Two Story Structure with Hallways. Technical report, Ammendale, Maryland, 2009.

[51] P. Isola, J.Y. Zhu, T. Zhou, A.A. Efros, Image-to-image translation with conditional adversarial networks, Proceedings - 30th IEEE Conference on Computer Vision and Pattern Recognition, CVPR 2017. 2017-Janua (2017) 5967–5976. https://doi.org/10.1109/CVPR.2017.632.

[52] Ministry of Housing and Urban-Rural Development of the People's Republic China, GB 50084-2017: Code for design of sprinkler systems, Ministry of Housing and Urban-Rural Development of the People's Republic China, 2017.

Appendix A. Supplementary data

Fig. A1 shows the applied floorplans in training and testing datasets, while the numbers are 51 (75%) and 17 (25%), respectively. For each floorplan, two different fire locations and ceiling heights are simulated. Fig. A2 shows the result of cell sensitivity study, while the reduction of cell size from 0.1 m to 0.05 m has no significant impacts on the gas temperature and velocity profiles. Fig. A3 presents the generated temperature fields by different deep learning algorithms for a new building floorplan. It shows that GAN model can better reproduce the transient flow patterns with higher accuracy. Fig. A4 compares the actual (CFD model) and predicted (GAN) ceiling fields at different timesteps on some testing cases. It demonstrates that proposed GAN model can provide comparable results to the CFD model for a given building floorplan.

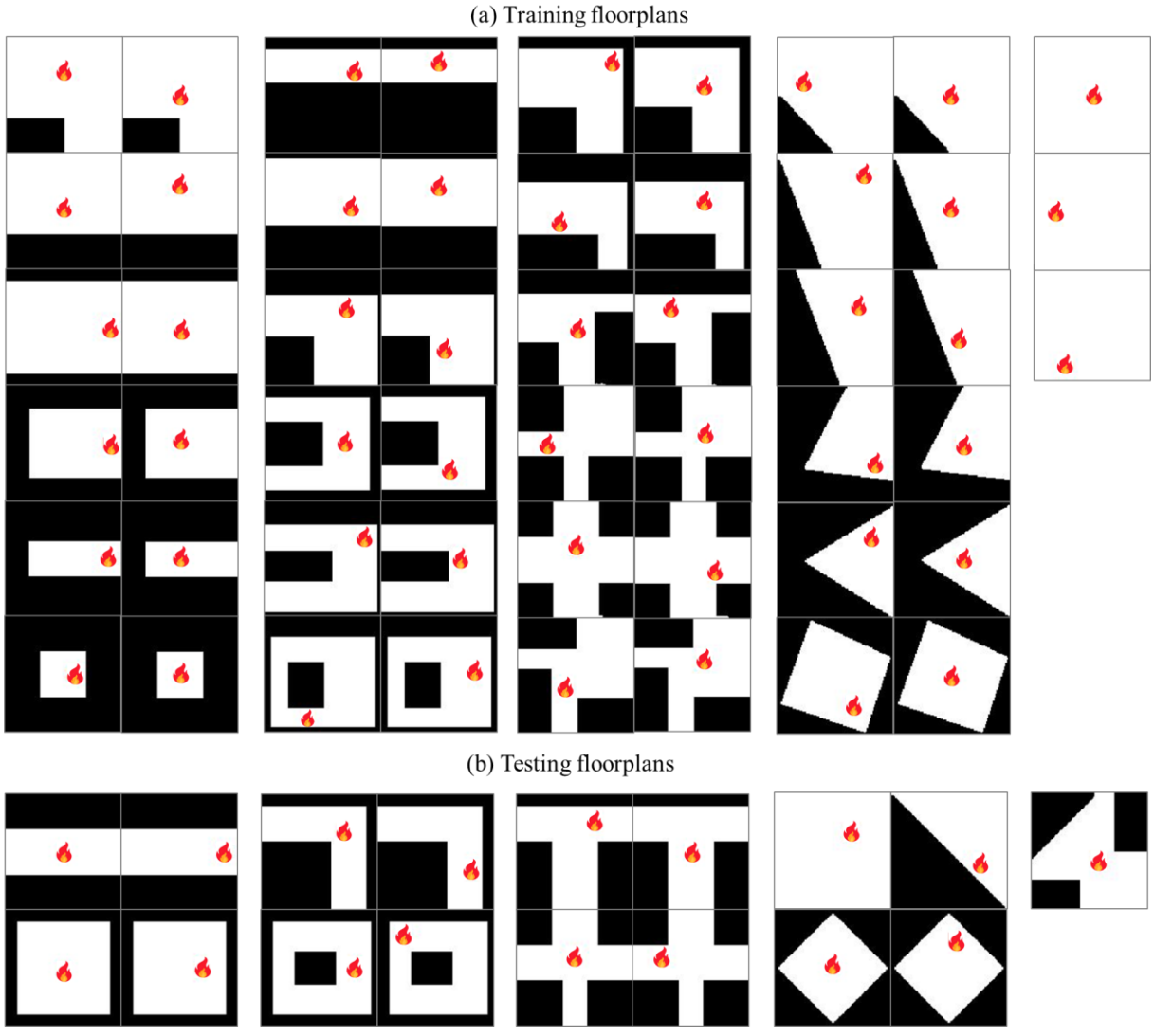

Fig. A1. Floorplans with fire location used for model (a) training and (b) testing, where the fire location (red), indoor space (white) and outdoor area (black) are presented.

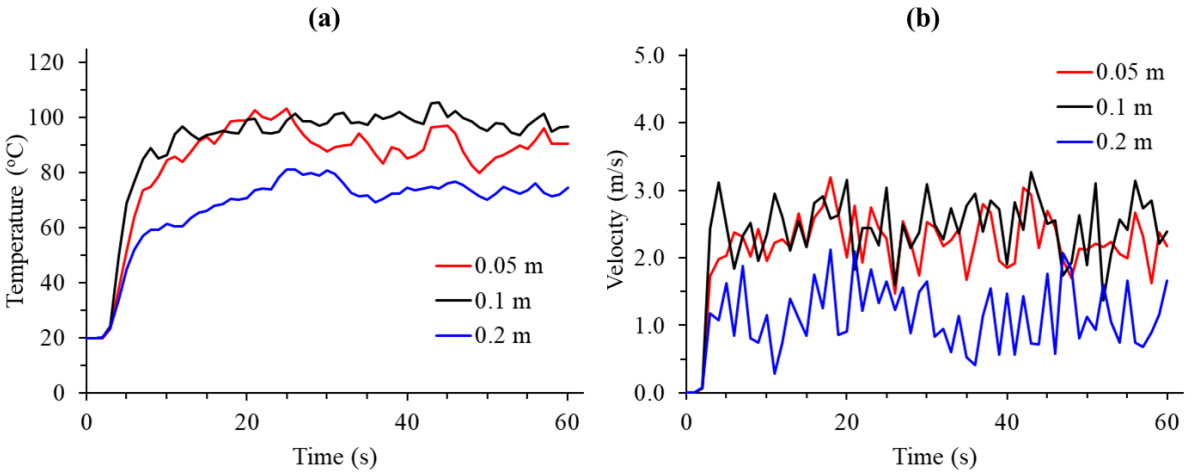

Fig. A2. Cell sensitivity analysis: (a) temperature and (b) velocity profiles at 2 m distance from fire centre.

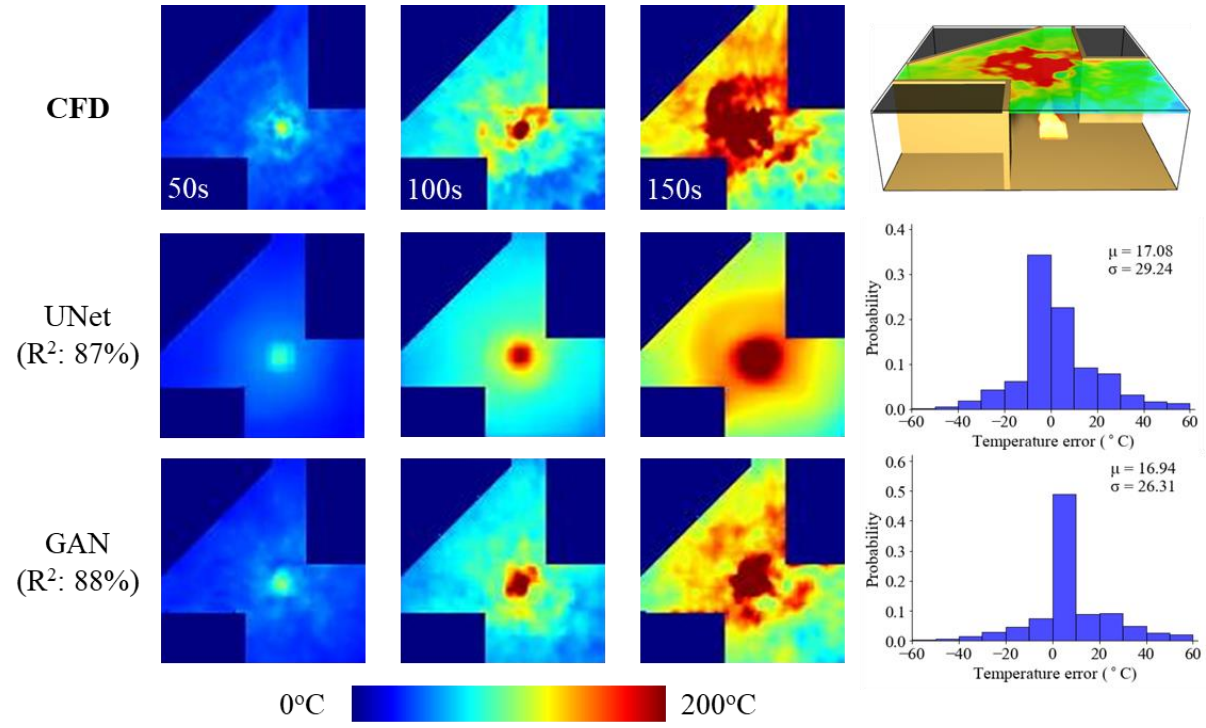

Fig. A3. Comparison of the generated temperature fields by different deep learning algorithms for a testing case.

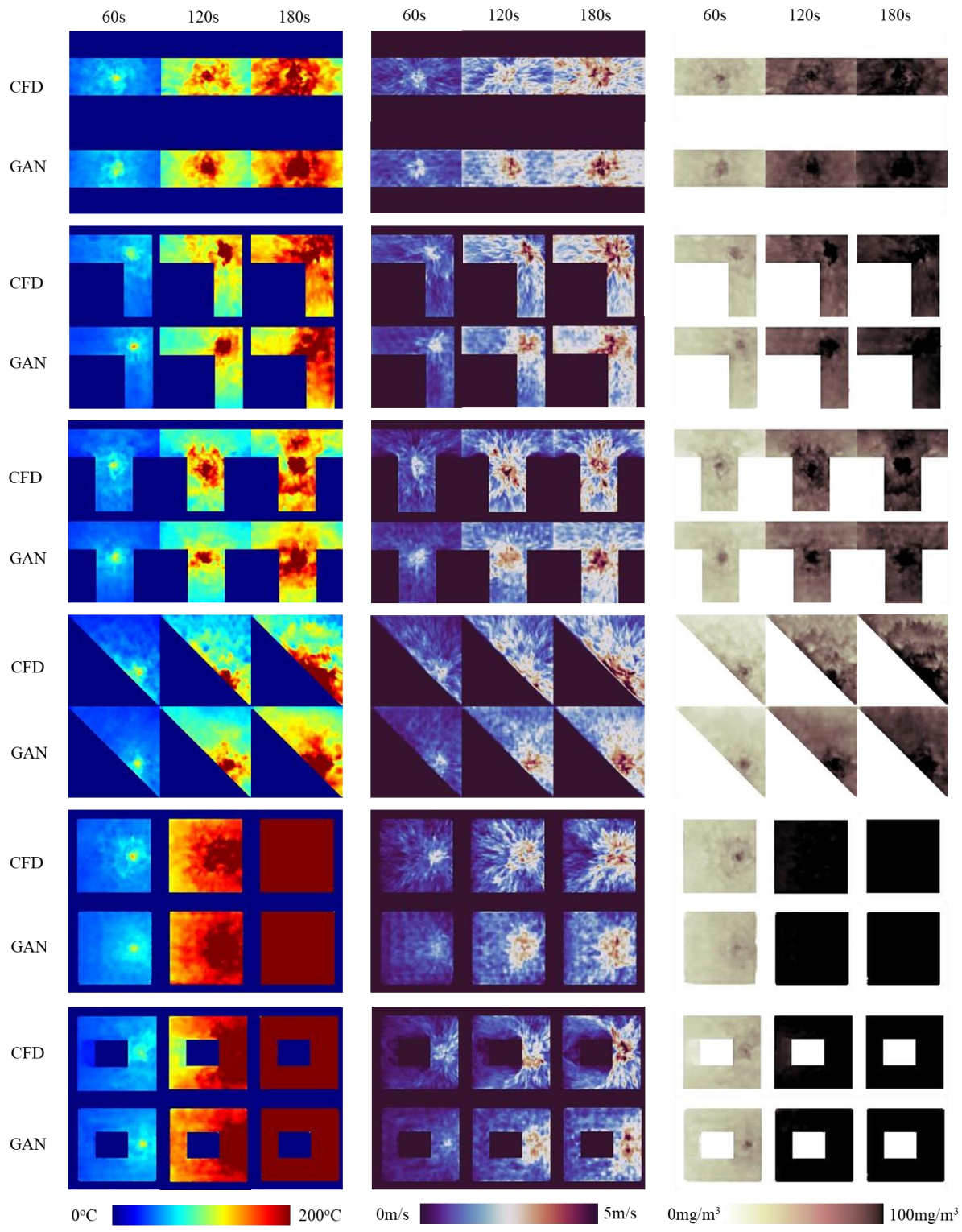

Fig. A4. Performance of GAN model on some testing cases.